SAND2012-7959P

# Nanostructured Electrode Materials for Lithium-Ion Batteries

Nicholas S. Hudak
Advanced Power Sources Research & Development
Sandia National Laboratories
Albuquerque, New Mexico, U.S.A.

Abstract

The use of nanostructured materials in lithium-ion batteries is reviewed with discussion of commercialization or potential for commercialization. Nanomaterials have the advantages of shorter distances for transport of ions or electrons and accommodation of strains associated with lithium insertion. These advantages enable the use of high-capacity electrode materials and offer the possibility of improved rate capability or cycle life. Nanostructuring has enabled the use of inexpensive, low-conductivity electrode materials, such as lithium iron phosphate and lithium titanate, and has resulted in the commercialization of batteries with these materials. Conversion-type electrode materials and lithium alloys, which offer significantly higher charge-storage capacity compared to conventional intercalation-type materials, have also been enabled by nanotechnology. The use of carbon nanostructures and carbon-based nanocomposites in lithium-ion electrodes is also discussed.

Keywords: nanotechnology, nanomaterials, lithium, conversion, alloy

## Introduction

Shortly following the widespread commercialization of lithium-ion batteries as power sources in portable electronic devices, nanotechnology came to the forefront of research and development in materials science. Nanostructured materials, which have dimensions on the order of 100 nanometers or less, have unique properties that are often significantly different from their bulk (or micron-scale) counterparts. Because of these unique properties, the use of nanomaterials in lithium-ion battery electrodes offers the potential for improved performance in terms of charge-storage capacity, rate capability, and cycle life. Increasing capabilities for synthesis of electrode materials as nanoparticles, nanocrystallites, or nanocomposites has resulted in an explosion of research activity in this area and, in several cases, commercialization of batteries containing nanostructured electrodes.

Nanostructured materials have several advantages that make them appropriate for lithium-ion electrodes.[1] Nanoparticles or nanocrystallites are smaller than bulk materials and thus require shorter distances for transport of electrons or lithium ions. This can result in enhanced rate capability (and thus power density) in conventional electrode materials or the ability to use insulating materials that would otherwise exhibit extremely limited performance. Another advantage is that nanoscale particles or crystals can more easily accommodate the strains associated with lithium insertion (via intercalation or phase transformation). For intercalation materials, this means there is a larger range of composition over which lithium intercalation occurs, which results in larger reversible capacity. The strain accommodation in nanomaterials also enables the use of high-capacity materials that undergo phase transformation upon lithium insertion. Nanomaterials also have important disadvantages that must be considered when they are used in lithium-ion electrodes. Nanoparticles have extremely high surface area and low density. The high surface area results in a higher likelihood of surface reactions, which often involve irreversible lithium consumption upon initial charge or discharge. Because of the low density of nanoparticle clusters, the higher gravimetric capacities often achieved by nanomaterials can be accompanied by lower volumetric capacity ("capacity" as it is used hereafter refers to specific gravimetric capacity). Another important disadvantage to be considered is that the synthesis of nanomaterials is often difficult and may be prohibitively expensive.

Detailed review articles on the use of nanomaterials for lithium-ion batteries[1-3] or for energy storage in general[4, 5] have been published in recent years. More focused reviews examine the use of nanomateri-

als in lithium-ion electrodes[6, 7] and specifically in positive[8] or negative[9] electrodes. The review presented here is not comprehensive and is intended to give an overview of the use of nanostructured materials in electrodes for lithium-ion batteries. The references cited here are early, illustrative, or highly-cited examples of the concepts. Synthesis of electrode materials is not covered here; the reader should consult the citation of a particular example for synthesis details. The most prominent examples of application or commercialization are given here, but a more detailed description of commercialization, including patent analysis, was given in a report by Kuyate and Patel.[10]

Nanoscale effects in intercalation-based electrode materials

Conventional active materials in positive electrodes of lithium-ion batteries are metal oxides that accommodate lithium via the intercalation mechanism. Intercalation involves the insertion of lithium into unoccupied sites in the crystal lattice, thus resulting in a small change to the unit cell volume and reversibility on the order of hundreds or thousands of cycles. The most common intercalation materials for positive electrodes are $LiCoO_2$, which has a two-dimensional layered structure, and $LiMn_2O_4$, which has a three-dimensional spinel structure. Nanoparticulate or nanocrystalline versions of these materials have been examined with the hope of achieving enhanced capacity, rate capability, or cycling performance.

An early example showed that $LiMn_2O_4$ could be prepared in nanoparticulate form using citrate solution with ethanol dehydration.[11] This is contrast to the conventional solid state synthesis route, which produces submicron- to micron-sized particles. $LiMn_2O_4$ particles with ~100-nm size exhibited higher delithiation and lithiation capacities (for the lithium-deficient composition, $Li_{1-x}Mn_2O_4$) in the first cycle compared to micron-sized particles produced by solid-state synthesis.[11] Particles with smaller average size, around 50 nm, exhibited lower capacities and worse cycling. These smaller particles had defective morphology and an absence of structural ordering during delithiation, which resulted in a different insertion mechanism and sloping voltage profiles (the absence of discernible plateaus). Kang et al. addressed the 3-volt region ($Li_{1-x}Mn_2O_4$) of spinel manganese oxide, which suffers from poor cycling in bulk crystalline form.[12] In this case, ball-milling of the bulk sample resulted in nanograin structure, higher manganese oxidation state, and stable cycling capacity in the 3-V region. The authors concluded that a critical grain size in the nanometer range allowed for stable cycling around 3 V vs. $Li/Li^+$ but at the expense of lower capacity in the 4-V region.

Nanostructuring has also proved effective in improving the rate capability of positive electrodes in lithium-ion batteries. This is mainly due to the decreased diffusion distances required for electrons and lithium ions in nano-sized crystals or particles. Size-controlled synthesis of $LiCoO_2$ was achieved through hydrothermal reaction and produced samples with average crystal sizes between 6.0 nm and 17 nm.[13] Samples with lower crystallite sizes exhibited higher irreversible capacity (during initial delithiation) and lower reversible capacity, especially when compared to bulk crystalline $LiCoO_2$. However, as shown in Figure 1a, the 17-nm sample showed an advantage in capacity compared to bulk $LiCoO_2$ when cycled at extremely high rate (100C, or 100 theoretical charges per hour). At this rate, the nanocrystalline sample achieved over 70 mAh $g^{-1}$. The nanocrystalline samples showed no advantage at rates of 50C and below. It is also worth noting, as shown in Figure 1b, that the nanocrystalline samples showed a more sloped voltage profile and the absence of a plateau during lithiation. This was attributed to the increased importance of surface reaction, disordered structure, and distribution of the site energy for reaction with lithium.[13] In the case of spinel $LiMn_2O_4$, Hosono et al. showed that single crystalline nanowires had a distinct advantage in rate capability over several bulk samples and over a wide range of rates (0.8C to 170C).[14] The nanowires, with a diameter of 50-100 nm, achieved capacity over 80 mAh $g^{-1}$ at the extremely high rate of 170C. This capacity is 67% of the theoretical value and was compared to *ca.* 40 mAh $g^{-1}$ achieved in commercial $LiMn_2O_4$ materials under the same conditions.[14] Despite the effectiveness demonstrated in improving rate capability, any decision to utilize such nanostructuring strategies in a commercial system would require consideration of the added cost of nanomaterials synthesis.

The use of nanomaterials has also been used to increase the amount of lithium intercalation in metal oxides whose bulk crystalline forms have limited capacity. Nanoparticulate forms of β-$MnO_2$,[15] α- and γ-

$MnO_2$,[16] α-$Fe_2O_3$,[17] and α-$LiFeO_2$[18, 19] exhibited intercalation capacity in voltage ranges above 1.5 V vs. $Li/Li^+$, where previous studies of bulk forms of these materials exhibited little to no intercalation capacity. An example of this is shown in Figure 2 for α-$Fe_2O_3$, which is a comparison of nanoparticles (~20 nm) to bulk crystalline particles (100-500 nm).[17] The voltage profile for lithiation of the nanoparticles exhibits a plateau around 1.6 V vs. $Li/Li^+$ that is not present in the profile of the bulk material. The lower plateau, below 1 V, is present for both materials and corresponds to the conversion to lithium oxide and metallic iron (see section on conversion materials below). *In situ* XRD results confirmed that the upper plateau in the nanomaterial corresponded to an intercalation mechanism. The authors also determined that this size effect was independent of lithium insertion rate. They concluded that the nanosized particles more easily accommodate strain (volume expansion) caused by intercalation before being forced to fully convert into lithium oxide and iron. Despite these interesting observations and the dramatic nanosized effects, the voltage ranges of these materials (2.5-3.5 V for $MnO_2$ and 1.5-2.5 V vs. $Li/Li^+$ for the iron oxides) are too low to be competitive with conventional materials for positive electrodes.

Nanostructured lithium metal phosphates for positive electrodes

The use of $LiFePO_4$ and other metal phosphates as positive electrodes in lithium-ion batteries was enabled by nanotechnology. Because these materials have intrinsically low ionic and electronic conductivity, the use of nanoparticles or particles coated with nanoscale conductive films is necessary to reach full charge-storage capacity. Electrode materials based on iron or other high-abundance metals are attractive because of low cost and long-term availability, so $LiFePO_4$ is a promising alternative to $LiCoO_2$ for positive electrodes. Theoretical capacity for full delithiation of $LiFePO_4$ is 170 mAh $g^{-1}$, which is another advantage over $LiCoO_2$ (140 mAh $g^{-1}$). The lithiation-delithiation reaction of $LiFePO_4$ is centered around 3.45 V vs. $Li/Li^+$,which is lower than that of $LiCoO_2$ and results in lower energy density. However, the lower potential is considered an advantage in terms of safety because the range of thermodynamic stability for typical lithium-ion battery electrolytes (cyclic and linear alkyl carbonates with $LiPF_6$ salt) is 1.5-4.5 V vs. $Li/Li^+$.[20, 21] Electrodes that are well within this range avoid dangerous side reactions and gas evolution, and cells that contain such electrodes can be charged at higher rates without approaching the stability limits. The use of $LiFePO_4$ as a positive electrode material has been reviewed extensively,[22-26] including reviews with focus on synthesis procedures[27] and carbon coating.[28]

Electrochemical delithiation of $LiFePO_4$ and lithiation of $FePO_4$ was first reported in 1997 by Goodenough and co-workers.[29] The cycling mechanism is not intercalation-based and requires phase transformation between $LiFePO_4$ and $FePO_4$. However, the structural similarity between the two phases results in a high degree of reversibility.[25] Despite the promise of efficient cycling, only ~0.6 lithium ions per iron atom were able to be inserted or extracted, and the full capacity of 170 mAh $g^{-1}$ was not achieved.[29] The problem was attributed to extreme rate limitations from the intrinsically low conductivity of the material. The advantages of nanostructure became apparent when nanocomposites of carbon and $LiFePO_4$ were introduced and exhibited capacities much closer to theoretical values.[30, 31] Nazar and co-workers concluded that synthesis with a carbon precursor and reduction of particle size to the submicron range were both necessary for improved performance.[30] Armand and co-workers found that similar performance improvements could be achieved by heat-treating the as-synthesized $LiFePO_4$ in the presence of a carbon source to create carbon-coated particles.[31] The presence of carbon facilitated electron- and ion-transport between particles, and the decreasing of particle size reduced the transport distances required. Various carbon-coating strategies were subsequently explored and optimized.[28] Another strategy that produced greatly improved conductivity was the doping of $LiFePO_4$ with a small percentage of other cations, e.g. $Nb^{5+}$ or $Zr^{4+}$.[32] Further examination of $LiFePO_4$ determined that neither carbon coating nor doping were necessary, rather that appropriate particle size with narrow size distribution and mild thermal treatment could produce similarly competitive performance.[33] Using this strategy, particles with average size of 140 nm were utilized to achieve stable cycling at 150 mAh $g^{-1}$ for hundreds of cycles. Further reduction of the particle size produced electrode behavior that resembled the intercalation mechanism, with a sloping voltage profile and gradually changing lattice parameters in the crystal structure.[34, 35] This was an im-

portant observation for nanoscience, in general, as it demonstrated conclusively that particle size in the nanometer range could have a great effect on reaction mechanism. Nevertheless, the carbon coating is still considered necessary as it makes the $LiFePO_4$ less sensitive to air, preventing $Fe^{2+}$ from oxidizing to $Fe^{3+}$.[24] Stability of electrode materials in air is necessary for ease of handling and mass production.

Examination of other lithium metal phosphates, such as $LiVOPO_4$,[36, 37] $LiMnPO_4$,[38-40] and $LiCoPO_4$[41, 42] accompanied the development of lithium iron phosphate (LFP) electrode materials. However, the low cost, excellent performance, and safety advantages of nanostructured LFP have made it the phosphate material of choice and the focus of intense research and development in the industrial sector. It has become the most widely commercialized nanomaterial for lithium-ion electrodes, and is intended mainly for use in electric vehicle batteries. The worldwide commercial importance of LFP is evident in the amount of companies involved in its development and production. Hydro-Québec originally obtained exclusive license on the Goodenough's patent for this family of materials. Hydro- Québec later partnered with the University of Montréal and Centre National de la Recherche Scientifique (CNRS) to spin off the company Phostech Lithium, Inc., based in Canada.[43] Phostech later became a wholly-owned subsidiary of Süd-Chemie AG (Germany) and the team planned to ramp up production to 2500 tons of LFP per year in 2012 with electric vehicles as the target application.[44] BASF Corporation[45] and LG Chem, Ltd.[46] have also entered into agreements with Hydro-Québec and Süd-Chemie, respectively, for mass production of LFP. Concurrent with this development, A123 Systems,[47] Valence Technology, Inc.,[48] and Saft[49] developed their own processes for LFP synthesis and integration into battery systems. Various patent disputes among some of these parties have been or are in the process of being settled,[50, 51] which also underscores the commercial importance of this material. Aside from application in electric vehicles, LFP is also being considered for grid-scale energy storage[45, 46, 52] and for military applications.[49, 53]

Titanium-based nanomaterials for negative electrodes

Various titanium-based compounds have been utilized as negative electrodes in lithium-ion batteries as alternatives to carbon-based intercalation electrodes. For these compounds, mainly $Li_4Ti_5O_{12}$ and various forms of $TiO_2$, lithium insertion and extraction occurs between 1.5 V and 2.0 V vs. $Li/Li^+$. This higher potential range results in lower cell voltage (and lower energy density) compared to cells with carbon-based negative electrodes operating around 100 mV vs. $Li/Li^+$. However, the higher potential is well within the thermodynamic stability limit of typical electrolyte solutions, so titanium-based negative electrodes largely avoid electrolyte decomposition and harmful side reactions. They can also be cycled at high rates without the danger of lithium plating, which gives them a great safety advantage over conventional carbon electrodes. Because of inherent transport limitations, titanium oxide electrode materials must be nanostructured to achieve full capacity and competitive cycling performance. The use of titanium-based compounds for lithium-ion electrodes was reviewed by Yang et al.[54] and Zhu et al.[55]

Lithium titanate spinel, with the structure $Li_4Ti_5O_{12}$, is similar to lithium iron phosphate in that it cycles between two phases with very similar crystal structure. Insertion of lithium into $Li_4Ti_5O_{12}$ forms $Li_7Ti_5O_{12}$ (theoretical capacity 175 mAh $g^{-1}$) at 1.55 V vs. $Li/Li^+$ and causes negligible volume change, which results in a high degree of reversibility.[56] Following initial reports of synthesis and electrochemical activity,[57] Grätzel and co-workers demonstrated that nanocrystalline and nanoparticulate versions of the material were far superior than micron-sized versions in terms of rate capability.[58, 59] Following this advance, the material was commercialized by Altair Nanotechnologies, Inc. (AKA Altairnano) for use in cells and battery packs with the main advantages of extended cycle life and safety at high charging rates. Altairnano's cells and batteries contain $LiCoO_2$ or $LiMn_2O_4$ as positive electrode materials, and the intended applications are electric vehicles and electric grid integration.[60] Company literature shows that the cells can undergo 9,000 cycles at full depth-of-discharge and a rate of 20C (20 theoretical charges or discharges per hour) before dropping to 80% of the initial capacity. There is also other commercial interest in lithium titanate materials for batteries. Hydro-Québec and Technifin recently entered into a collaboration agreement to develop lithium titanate-based batteries,[61] and the NEI Corporation manufactures and sells nanoscale and micron-scale versions of lithium titanate under the trade name Nanomyte®.[62]

Various polymorphs of titanium dioxide have also exhibited the ability to electrochemically cycle with lithium.[54] The promise of these materials is their theoretically higher capacity (336 mAh $g^{-1}$ for $TiO_2 \rightarrow LiTiO_2$) than lithium titanate, but performance has not proved to be competitive. Initial demonstration showed that 0.5 lithium ions per titanium atom could be cycled around 1.8 V vs. $Li/Li^+$ in nanocrystalline anatase-type $TiO_2$.[63] In general, smaller particle size and crystallite size, down to the nanoscale, resulted in higher amounts of lithium insertion.[64, 65] The use of anatase nanotubes was also explored but did not produce any dramatic results in terms of improved capacity or rate capability.[66, 67] Nanowires[68, 69] and nanotubes[70] made of $TiO_2$-B (bronze-type polymorph) exhibited slightly higher capacities, but it is unknown whether the long-term cycling of these materials could be competitive with lithium titanate. Furthermore, lithium insertion for most of the $TiO_2$ materials required broad ranges (on the order of 1 volt) to achieve full capacity, which is in sharp contrast to the titanate materials, which have all exhibited flat voltage profiles and low hysteresis.[54]

Conversion electrodes

Reversible cycling of so-called conversion electrodes with lithium was enabled by the use of nanostructured materials. Conversion electrodes are those that require breaking and re-forming of bonds (and the concomitant rearrangement of crystal structure) during cycling with lithium. This is in contrast with the more conventional intercalation electrodes ($LiCoO_2$, $LiMn_2O_4$, graphite, etc.), which insert lithium into interstitial spaces between atoms, causing no change to the crystal structure and only small increases in the unit cell volume. A schematic comparison between intercalation-type and conversion-type electrode reactions is shown in Figure 3.[71] While the intercalation electrodes can only accommodate up to one lithium ion per metal atom, limiting their capacities to less than 250 mAh $g^{-1}$, the conversion electrodes can react with up to three lithium ions per metal atom, allowing capacities greater than 700 mAh $g^{-1}$. Conversion materials are typically transition-metal oxides, fluorides, nitrides, phosphides, or sulfides. With the exception of the fluorides, these materials react with lithium at low potentials (0-2 volts vs. $Li/Li^+$) and are thus intended for negative electrodes in lithium-ion batteries. The initial cycling demonstration of various metal oxide nanoparticles by Poizot et al.[72] sparked extensive research efforts in conversion materials. The use of conversion materials in electrodes for lithium-ion batteries was reviewed initially by Malini et al.[73] and in great detail by Cabana et al.[74]

It was long known that metal oxides could electrochemically react with lithium at low potential to form a mixture of lithium oxide and metallic particles.[75] However, the reversibility of this reaction was not certain until Poizot et al. demonstrated cycling of CoO, NiO, and FeO nanostructures as the active electrode materials in lithium half-cells.[72] The potential vs. composition curves of these cells are shown in Figure 4 along with the cycling performance. For the initial lithiation, each of these materials reached near-theoretical capacity for the complete two-electron reduction of the metal. As shown in Figure 4, cycling of these oxide materials occurs mainly in the potential range of 1-3 volts vs. $Li/Li^+$. Thus, the benefit of higher capacity compared to conventional carbon-based negative electrode materials is somewhat offset by the higher reaction potential of conversion materials (which would result in lower cell voltage and possibly lower energy density). The lithiation and cycling of $Co_3O_4$ in the same study (see Figure 4) also proved that divalent *and* trivalent reduction of the metal was possible to achieve even higher capacity (nearly 1000 mAh $g^{-1}$ at the 25$^{th}$ cycle).[72] Further examination of $Co_3O_4$ revealed that the surface area and crystallite size (in the 15-100 nm range) have a strong influence on the reaction path to formation of $Li_2O$ and Co metal.[76] TEM images showed that electrochemical lithiation of $Cu_2O$ microparticles produced nanograins of copper metal embedded in a $Li_2O$ matrix, and the nanograin structure was retained upon delithiation.[77] These types of nanodomain structures are necessary to achieve efficient cycling in conversion materials. This is due to the radical phase transformations that occur during lithiation and delithiation; nanostructure allows for the relaxation of strain and provides shorter distances for electron and ion transport.

Following these initial demonstrations of conversion materials, a flurry of research into various nanostructures occurred. Yuan et al. showed that $Co_3O_4$ nanoparticles (as opposed to microparticles with

nanocrystalline structure) could be efficiently cycled, but performance degraded as particle size was reduced below 37 nm.[78] The research community also showed interest in $Co_3O_4$ nanowires synthesized by various procedures,[79-81] but these materials offered no improvement in performance over the original demonstration shown in Figure 4.[72] $Fe_3O_4$ and $Mn_3O_4$ electrodes were studied as lower-cost alternatives and face the same challenges as the other conversion oxide materials. Nanospindles,[82] nanocrystals,[83] nanowires,[84] and nanocomposites[85] made of $Fe_3O_4$ exhibited relatively stable cycling at 800-1000 mAh $g^{-1}$ and reasonable rate capability. $Fe_2O_3$ nanoflakes,[86] $Fe_2O_3$ nanotubes,[87] and $Mn_3O_4$ nanoparticle-graphene composites[88] were also explored, and all exhibited comparable performance to the $Fe_3O_4$ structures. Nanostructures of transition-metal nitrides, sulfides, and phosphides have been less studied than those of the oxides, and they are covered in the review by Cabana et al.[74] In the absence of direct comparison between these varied nanostructures, it is difficult to tell which, if any, is the most appropriate for commercialization and if any could be incorporated into conventional battery manufacturing processes.

Transition-metal fluorides have also gained prominence as a type of conversion material that can be used in the positive electrodes of lithium-ion batteries. Electrochemical reaction of metal fluorides with lithium occurs at a higher potential, around 3 V vs. $Li/Li^+$, because of the extreme ionic character of the metal-fluorine bond.[71] As with the other conversion materials, nanostructuring of metal fluorides is essential for cycling in lithium-ion batteries. Badway et al. initially showed that iron fluoride ($FeF_3$) could be reversibly cycled at near-theoretical capacity by reducing the crystallite size to 25 nm and by combining with carbon in a nanocomposite.[89] This concept is illustrated in Figure 5, which shows the voltage profile of cycling $FeF_3$ electrodes with crystallite sizes of 102 nm and 25 nm. Also shown here is the higher potential range of fluoride electrodes, with reduction and oxidation curves centered around 3.5 V vs. $Li/Li^+$. Further increases in cycling capacity (up to 500 mAh $g^{-1}$) were achieved by altering the solid-state synthesis procedure, and 680 mAh $g^{-1}$ was achieved with the use of a $CrF_3$-carbon nanocomposite.[90] The introduction of oxygen to the structure to create iron oxyfluoride (FeOF) resulted in increased cycling stability at the expense of reversible capacity.[91] While these fluorides are among the highest-capacity positive electrode materials ever observed, their major obstacles to commercialization are extreme rate limitations and voltage hysteresis during cycling. They could thus most appropriately be utilized in applications that require high specific energy density but do not require high power density or energy efficiency.

Lithium alloys for negative electrodes

Nanostructured materials enable the use of lithium alloys as negative electrodes in lithium-ion cells. The electrochemical alloying of certain metals with lithium at room temperature in organic electrolyte solutions was first demonstrated by Dey.[92] At low potentials, these metals electrochemically react with lithium to form alloys of distinct stoichiometric composition. Similar to the conversion-type electrode reactions discussed in the previous section, electrochemical alloying reactions require phase transformation, significant rearrangement of atoms, and large changes in volume (strain). The de-alloying and continued cycling of these electrodes results in disintegration or pulverization of active particles. In other words, a lithium-alloy particle is unable to accommodate the strain associated with removal of a large amount of lithium, and the particle responds by separating into smaller, separate sub-particles. Sub-particles that become isolated from the rest of the electrode are no longer active, and the result is a loss in cycling capacity. In many cases, nanoparticles and thin films of nanometer thickness can better accommodate the strain of de-alloying and cycling. Nanostructured lithium-alloy electrodes demonstrated the best ability to obtain theoretical capacity and retain higher capacity with continued cycling. Lithium-alloy electrodes have been the subject of extensive research in the last decade, and they were reviewed in detail by Larcher et al.,[93] Park et al.,[94] and Zhang.[95] The mechanisms of electrochemical alloying and de-alloying with lithium were also reviewed by Zhang.[96]

The first demonstrations of electrochemical lithium-alloying at room temperature showed that this process occurs with Sn, Pb, Al, Au, Pt, Zn, Cd, Ag, Mg, Bi, and Sb and does not occur to any measurable extent with Ti, Cu, Ni, or stainless steel.[92, 97] Silicon also electrochemically alloys with lithium, and it has

the highest gravimetric capacities (theoretical and observed) amongst this group.[93-95] The most lithiated lithium-silicon alloy known to exist at room temperature is $Li_{22}Si_5$, which has a theoretical lithium-storage capacity of 4200 mAh $g^{-1}$ (relative to silicon mass). This value is an order of magnitude higher than the theoretical capacity of carbon-based electrodes, which are commonly used as negative electrodes in commercial lithium-ion batteries. Silicon has thus become the most extensively studied of the lithium-alloy electrodes, and it is the lithium-alloy electrode most often considered for commercialization. Lithium-silicon electrodes for lithium-ion batteries have been reviewed in detail with particular emphasis on nanostructured electrodes.[98, 99]

The use of nanocomposites and nanomaterials enabled the extended cycling of lithium-silicon electrodes. In one of the earliest demonstrations of this, a composite of silicon nanoparticles and carbon black was used as the active material in lithium half-cells.[100] The nanomaterials significantly outperformed a micron-scale composite of silicon and carbon in terms of cycling capacity. While the micron-scale material decreased from 2900 mAh $g^{-1}$ to under 500 mAh $g^{-1}$ in only 5 cycles, the nanomaterial exhibited 1300 mAh $g^{-1}$ at the 22$^{nd}$ cycle. However, the capacity was still exhibiting a significant decrease at this point in the cycle life, and subsequent research in lithium-silicon electrodes has addressed ways of nanostructuring such electrodes to obtain both high capacity and stable cycling. Silicon films of nanoscale thickness have been used to demonstrate the ability to retain high capacity after tens, hundreds, or thousands of cycles.[101-104] Vacuum-deposited silicon films of 50-nm thickness retained 3600 mAh $g^{-1}$ capacity after 200 cycles at 2C rate (two theoretical charges or discharges per hour). Thus, silicon has an intrinsic ability to reversibly cycle near its theoretical capacity, but this ability is highly dependent on electrode structure. It has not yet been possible to translate the cycling performance of nanosized films to that of a three-dimensional porous electrode with a high amount of capacity per unit area. Transport issues inevitably come into play in the design of lithium-alloy electrodes, and capacity and reversibility are often limited by the electronic or ionic conductivity of the composite electrode rather than that of the individual electrode components.

Silicon nanowires were introduced as a way of obtaining enhanced interparticle contact (and thus transport) while retaining the benefits of nanosize strain relaxation in the radial direction.[105, 106] While these early reports had a limited amount of capacity and cycling data, Cui and co-workers renewed interest with their fabrication and testing of vapor-deposited silicon nanowires on stainless steel substrates.[107] The wires, with an average diameter of 89 nm, maintained good contact with the substrate upon cycling and steady capacity above 3000 mAh $g^{-1}$ for the first 10 cycles at C/20 rate (20 hours per theoretical charge or discharge). However, continued cycling at C/5 showed a steady decrease in capacity to 2000 mAh $g^{-1}$ after 80 cycles.[108] Continued improvements in cycling stability are needed for silicon electrodes to be commercially competitive with carbon-based negative electrodes in lithium-ion batteries. Research continues in many related areas, including nanoparticle size optimization[109] and *in situ* investigation of the lithiation-delithiation process.[110] Several companies promote upcoming products based on lithium-ion batteries with silicon electrodes. These include Nexeon (UK), who advertises silicon nanowire batteries[111] based on earlier work by Green et al.[112]; 3M, whose website publicizes cycling and rate data for batteries with silicon-based negative electrodes[113]; and Amprius, which spun off from Yi Cui and co-workers' research at Stanford University.[114]

Lithium-alloy electrodes other than those based on silicon have been far less studied, but particular attention has been paid to tin, $SnO_2$, and aluminum. Tin forms the alloy $Li_{22}Sn_5$, which has a theoretical capacity of 990 mAh $g^{-1}$. Similar to the silicon alloy, lithium-tin has a sloping voltage profile mainly in the range of 0-1 V vs. $Li/Li^+$. Winter and Besenhard reviewed the early work on tin and tin-related compounds as lithium alloys.[115] As expected, scaling down the size of Sn particles to the submicron and nanoscale ranges has resulted in significant increase in cycling stability.[116, 117] Tin oxide ($SnO_2$) has also been studied as a less expensive variation in which lithium oxide is irreversibly formed upon initial lithiation. The resultant metallic tin then reversibly cycles with lithium in the stable oxide matrix. Nanofibers and nanoparticles showed decent performance and better cycling for smaller structures.[118, 119] However, it is unclear whether there is an advantage of any tin-based electrode over silicon, given the higher cost and lower capacity of tin. Aluminum, which forms the single alloy phase LiAl with lithium, has a theoretical

capacity of 990 mAh $g^{-1}$ and is cost-competitive with silicon. It is one of the few lithium-alloying materials that exhibited worse performance when scaled down to the submicron and nanosized ranges. This was observed for aluminum particles[120] and films[121] and was attributed to the formation of a rigid oxide layer on the surface.[122]

Nanostructured intermetallic alloys can also be used as active electrode materials in lithium-ion batteries. The benefit in this case is the addition of an inactive metal into the host metal, which helps to buffer the large strains upon lithium alloying and thus improve reversibility. The improvement in cycling performance is accompanied by a sacrifice in lithium-storage capacity. The characteristics of a large number of intermetallics for electrochemical lithium-alloying were compiled and reviewed by Zhang.[95, 96] This strategy has been applied to improve the cycling performance of aluminum nanostructures with lithium by adding small percentages of copper[123] or yttrium[124] to the host material. Even more prominent in the literature is the addition of transition metals to tin nanostructures to improve cycling performance.[125-127] The most studied of these materials has been amorphous Sn-Co nanoparticles, which exhibited enhanced capacity over crystalline and bulk counterparts[125] and was further enhanced with the addition of carbon.[126] Versions of this material were commercialized by SONY for the negative electrode in their Nexelion™ battery, which was rated at 30% higher capacity per volume relative to conventional lithium-ion batteries.[128] The early version of this product was intended for video cameras[128] while a more recent, larger version was aimed at personal computers.[129]

Carbon nanostructures as active materials in negative electrodes

Active materials in the negative electrodes of lithium-ion batteries are typically graphite or related forms of carbon, so it is not surprising that nanoscale forms of pure carbon have been explored in the hopes of achiever higher reversible capacity or enhanced rate capability. In bulk graphite, lithium intercalates between the layers in a series of discrete, ordered compositions (the staging phenomenon) with a maximum composition of $LiC_6$ (corresponding to 372 mAh $g^{-1}$). The resulting potential profile is characterized by a slope at low lithium content, two flat plateaus below 100 mV vs. $Li/Li^+$, and very low hysteresis owing to low resistivity and reaction overpotentials. The low potential has the advantage of high energy density (from high cell voltage) with the disadvantage of safety issues due to the possibility of lithium plating. The use of nanoscale forms of carbon has mainly resulted in increased cycling capacity at the expense of a disadvantageous potential profile (broad potential range and high hysteresis). These efforts were reviewed in detail by Kaskhedikar/Maier[130] and Su/Schögl.[131]

Carbon nanotubes are the quintessential nanomaterials and are considered for a wide range of applications due to their exceptional mechanical and electronic properties. The use of carbon nanotubes in lithium-ion batteries was reviewed by Landi et al.[132] Single-wall carbon nanotubes (SWNT) are single graphene tubules with diameters of several nanometers and lengths in the submicron to micron range. Gao et al. first explored the electrochemical insertion of lithium into SWNT.[133, 134] They observed reversible capacity of 600 mAh $g^{-1}$ upon initial cycling, which increased to 1000 mAh $g^{-1}$ when ball-milled SWNT was used. It was proposed that ball-milling induces disorder in the SWNT, which leads to increased sites for reaction and access to the inside of the tubes.[133] As shown in Figure 6, the potential profile of SWNT-Li cycling is characterized by broad voltage range (0-3 V vs. $Li/Li^+$), high hysteresis, and large irreversible capacity upon initial lithiation (probably due to electrolyte breakdown and solid-electrolyte-interphase formation on the high surface area). Qualitatively, Smalley and co-workers made similar observations with SWNT and lithium, but in their case the reversible capacity was 460 mAh $g^{-1}$.[135] The absence of distinct peaks in the cyclic voltammogram allowed them to rule out the staging mechanism for lithium insertion. Using *in situ* XRD as support, they proposed that the lithium ions intercalate between nanotubes in a bundle and disrupt the inter-tube binding.

Multiwall carbon nanotubes (MWNT) consist of graphitic sheets rolled in concentric cylinders and have also been examined for electrochemical insertion of lithium.[132] The potential profiles of MWNT lithiation and cycling were very similar to those of the SWNT studies: high irreversible capacity (mainly near 1 V vs. $Li/Li^+$ and thus attributable to electrolyte decomposition), broad voltage range of 0−3 V vs.

$Li/Li^+$, and high hysteresis (~1 volt or higher difference between lithiation and delithiation).[136-138] Reversible capacities ranged from 100-400 mAh $g^{-1}$, lower than those of the SWNT and not significantly higher than conventional carbon electrodes. Heat treatment of MWNT was shown to have a significant effect on electrochemical behavior; samples that were heat-treated to higher temperature or more highly graphitized tended to exhibit lower irreversible and reversible capacities and better cycling stability.[136-138] This was attributed to the lower surface area and lower amount of irregularities in the heat-treated samples.[136] Despite years of research into carbon nanotubes, more recent studies of lithium insertion and cycling still showed no significant advantage over the use of conventional micron-scale graphite or carbon particles in terms of capacity or rate capability. Electrodes made of these materials are still hindered by the problems of large irreversible capacity (which causes large consumption of lithium during initial battery charging), broad voltage range, and high voltage hysteresis.[139] A more appropriate application of carbon nanotubes in lithium-ion batteries is in the fundamental research studies of electrode reactions themselves. For example, Liu et al. performed an *in situ* TEM study of the electrochemical lithiation of graphitic layers in MWNT and were able to observe its effects on layer spacing and mechanics.[140] Such high-resolution imaging of the lithiation process is only possible with nanomaterials and could not be performed with conventional carbonaceous electrode materials.

Carbon nanofibers (CNF) are another type of nanostructure considered for lithium-ion electrodes. Yoon et al. argued that CNF could potentially be produced at a lower cost than conventional carbons because they are able to be graphitized at lower temperature.[141] CNFs that were highly graphitized exhibited evidence of staging phenomena, voltage profiles similar to those seen in commercial carbon electrode materials, and reversible capacities of 350-400 mAh $g^{-1}$. However, irreversible capacity on the first cycle was large (~300 mAh $g^{-1}$), and continued cycling was not shown. Electrospun CNFs were also examined but exhibited broader voltage profiles and similar irreversible capacity.[142, 143] Reversible capacity at 50 mA $g^{-1}$ rate was observed (greater than 400 mAh $g^{-1}$ for 50 cycles) but required a voltage range of 0−3 V vs. $Li/Li^+$ to achieve full capacity.[143]

Graphene has suffered from the same performance drawbacks as other carbon nanostructures in the negative electrode of lithium-ion batteries while being touted in the literature as a possible alternative to conventional carbons. Graphene is a single sheet of $sp^2$ hybridized carbon and can be envisioned as an exfoliated graphite layer or an "unzipped" carbon nanotube. The use of graphene in lithium-ion batteries was reviewed by Liang and Zhi,[144] Pumera,[145] and Brownson et al.[146] Graphene, like other carbon nanostructures, has the drawback of low volumetric capacity because of its high surface area and low density. For lithium cycling, graphene exhibited a broad potential range with high hysteresis and significant irreversible capacity in the first cycle[147-149] (again due to electrolyte decomposition on the surface around 1 V vs. $Li/Li^+$), and it showed decreasing capacity with continued cycling.[149-151] The charge-discharge voltage profile and cycling behavior of graphene are shown in Figure 7 compared to that of graphite. These curves are typical of all the carbon nanostructures above and show that a wide voltage range must be used to obtain full capacity (compared to graphite, which only requires a 0.5-volt range to obtain the great majority of the capacity).

The applicability of carbon nanostructures as active lithium-storage materials in batteries is called into question by their poor performance as demonstrated to date. The large irreversible capacity upon initial lithiation would require the use of a significantly larger positive electrode as a lithium source, which would result in lower overall energy density and possible transport limitations. The broad potential range (requiring as high as 3 V vs. $Li/Li^+$ for full delithiation) would also result in low energy density, and large voltage hysteresis causes low energy efficiency. It is likely that carbon nanostructures are more useful as conductive additives or as part of nanocomposites in electrodes rather than as active materials themselves.

Carbon-based nanocomposites

Aside from being considered as active lithium-insertion materials, carbon nanostructures can be combined with another active material to form a composite with higher conductivity or better cycling than the active material alone. This strategy was reviewed in detail by Su and Schögl.[131] The most common ex-

ample is the coating of a nanoscale layer of carbon on $LiFePO_4$ particles for improved conductivity as discussed above. In a related example, $LiFePO_4$ nanoparticles were also combined with graphene via mixture in suspension, and the composite exhibited improved capacity and rate capability compared to carbon-coated $LiFePO_4$ particles.[152] Various other strategies for combining lithium metal phosphates with carbon nanostructures to obtain enhanced conductivity have also been attempted.[153]

Another active material that is commonly combined with nanoscale carbon is silicon, which forms an alloy with lithium for negative electrodes, as described above. In this case, carbon may not only improve conductivity but can also buffer or confine volume changes upon lithiation and delithiation to obtain improved cycling. Silicon-carbon composites for lithium-ion electrodes were reviewed by Kasavajjula et al.,[99] but many more related attempts have since been made. Hertzberg et al. used a computational model to predict that stable cycling of silicon could be achieved by confining it in a rigid shell, thus preventing long-range pulverization.[154] The authors verified the model by fabricating and testing a nanocomposite structure consisting of a 300-nm diameter silicon tube enclosed in a slightly large carbon tube. Stable capacity was observed at 80 mA $g^{-1}$ for 250 cycles. The added weight of carbon resulted in capacity around 800 mAh $g^{-1}$, less than a quarter of theoretical capacity. Using a similar strategy, Kim and Cho observed higher capacities (> 2700 mAh $g^{-1}$) and less stable cycling in a nanocomposite consisting of a silicon rod of 4-nm diameter surrounded by an amorphous carbon layer of 1-2 nm thickness.[155] Conversely, Cui et al. demonstrated that similar cycling behavior could be achieved by using carbon nanofibers with thin layers of amorphous silicon deposited over the surface.[156] In 2009, Samsung Co. published a report of nanocomposites of silicon and carbon nanotubes (SWNT and MWNT variations).[157] This suggests there may be commercial interest in such materials, especially if they enable the use of high-capacity electrodes.

In terms of other lithium-alloying elements, carbon nanocomposites have been explored with tin and $SnO_2$ in attempts to improve their lithium-cycling behavior. Yu and co-workers synthesized unique nanocomposites composed of tin nanparticles embedded in carbon microtubes[158] and carbon nanofibers.[159] Both materials exhibited cycling behavior that was far superior to that of commercial tin nanopowder. Other nanocomposites that exhibited superior cycling behavior to tin or $SnO_2$ alone were carbon tubes (~200-nm diameter) filled with tin,[160] carbon-encapsulated hollow tin naparticles,[161] elastic carbon spheres filled with multiple tin nanoparticles,[162] tin nanoparticles embedded in a micron-scale carbon matrix,[163] and graphene-$SnO_2$ hybrid nanoparticles.[164, 165]

Oxide materials have also been combined with carbon to form nanocomposites with enhanced cycling performance and rate capability. Zhi et al. synthesized carbon-cobalt nanocomposites with various types of structures and oxidized them to form $Co_3O_4$-carbon nanocomposites.[166] The composites exhibited superior cycling stability at a rate of 0.2C compared to $Co_3O_4$ particles of 20-30 nm diameter. In another study, a composite of ~20-nm $Co_3O_4$ particles anchored on graphene sheets exhibited both superior cycling and rate capability to $Co_3O_4$ particles alone. Similarly, the reversible cycling of $Fe_2O_3$ as a conversion material was enabled by synthesizing it in the presence of graphene oxide to form a nanocomposite.[167] Capacities above 1000 mAh $g^{-1}$ for 50 cycles were observed. The authors concluded that the combined synthesis, rather than simply mixing $Fe_2O_3$ nanoparticles with graphene oxide, was necessary to achieve high-capacity cycling. Despite the impressive improvements achieved with these nanocomposites, the incorporation of carbon into conversion-type electrode materials has not addressed the issue of voltage hysteresis, which was observed as significantly with the nanocomposite electrodes as it was with the unaltered conversion electrodes. This, along with the complicated (and likely expensive) synthesis procedures required, calls into question the usefulness of nanocomposites in bringing conversion electrodes to the commercially-relevant sphere.

## Conclusion

Nanomaterials have made a significant impact on the science of lithium-ion batteries, especially when used in electrodes to achieve higher capacity, rate capability, or cycle life. Investment in this area has resulted in rapid development and commercialization of batteries containing lithium iron phosphate or

lithium titanate as electrode materials. The inherently low conductivity of these materials required that they be implemented in nanostructured form to exhibit competitive performance in terms of capacity and rate capability. Silicon is a higher-capacity alternative to carbon for negative electrodes, and its use in lithium-ion batteries was also enabled by nanostructuring. Silicon nanoparticles and nanocomposites appear to be the next nanomaterials slated for commercialization. Nanostructured conversion materials and carbon nanostructures have also been examined as alternative electrode materials, but the advantages they offer are as yet outweighed by performance limitations.

Acknowledgements

The author thanks Chris Orendorff and Summer Ferreira, both of Sandia National Laboratories, for helpful discussion. The author acknowledges the financial support of the Laboratory Directed Research and Development (LDRD) program at Sandia National Laboratories. Sandia National Laboratories is a multi-program laboratory managed and operated by Sandia Corporation, a wholly owned subsidiary of Lockheed Martin Corporation, for the U.S. Department of Energy's National Nuclear Security Administration under contract DE-AC04-94AL85000.

References

1. P. G. Bruce, B. Scrosati and J.-M. Tarascon, *Angewandte Chemie International Edition*, 2008, **47**, 2930-2946.
2. E. Stura and C. Nicolini, *Analytica Chimica Acta*, 2006, **568**, 57-64.
3. M. S. Whittingham, *Dalton Transactions*, 2008, 5424-5431.
4. A. S. Arico, P. Bruce, B. Scrosati, J.-M. Tarascon and W. van Schalkwijk, *Nat Mater*, 2005, **4**, 366-377.
5. J. Chen and F. Cheng, *Accounts of Chemical Research*, 2009, **42**, 713-723.
6. M. G. Kim and J. Cho, *Advanced Functional Materials*, 2009, **19**, 1497-1514.
7. L. F. Nazar, G. Goward, F. Leroux, M. Duncan, H. Huang, T. Kerr and J. Gaubicher, *International Journal of Inorganic Materials*, 2001, **3**, 191-200.
8. Y. Wang and G. Cao, *Adv Mater*, 2008, **20**, 2251-2269.
9. L. Ji, Z. Lin, M. Alcoutlabi and X. Zhang, *Energy & Environmental Science*, 2011, **4**, 2682-2699.
10. P. S. Kuyate and V. Patel, *Patent analysis and product survey on use of nanomaterials in lithium-ion batteries* http://www.nanowerk.com/spotlight/spotid=21950.php, Accessed September 12, 2012.
11. J. H. Choy, D. H. Kim, C. W. Kwon, S. J. Hwang and Y. I. Kim, *J Power Sources*, 1999, **77**, 1-11.
12. S.-H. Kang, J. B. Goodenough and L. K. Rabenberg, *Chem Mater*, 2001, **13**, 1758-1764.
13. M. Okubo, E. Hosono, J. Kim, M. Enomoto, N. Kojima, T. Kudo, H. Zhou and I. Honma, *Journal of the American Chemical Society*, 2007, **129**, 7444-7452.
14. E. Hosono, T. Kudo, I. Honma, H. Matsuda and H. Zhou, *Nano Letters*, 2009, **9**, 1045-1051.
15. W. P. Tang, X. J. Yang, Z. H. Liu and K. Ooi, *J Mater Chem*, 2003, **13**, 2989-2995.
16. F. Cheng, J. Zhao, W. Song, C. Li, H. Ma, J. Chen and P. Shen, *Inorganic Chemistry*, 2006, **45**, 2038-2044.
17. D. Larcher, C. Masquelier, D. Bonnin, Y. Chabre, V. Masson, J.-B. Leriche and J.-M. Tarascon, *J Electrochem Soc*, 2003, **150**, A133-A139.
18. J. Morales and J. Santos-Pena, *Electrochem Commun*, 2007, **9**, 2116-2120.
19. J. Morales, J. Santos-Peña, R. Trócoli, S. Franger and E. Rodríguez-Castellón, *Electrochim Acta*, 2008, **53**, 6366-6371.
20. J. B. Goodenough and Y. Kim, *Chem Mater*, 2009, **22**, 587-603.
21. K. Xu, *Chemical Reviews*, 2004, **104**, 4303-4418.

22. Z. Li, D. Zhang and F. Yang, *Journal of Materials Science*, 2009, **44**, 2435-2443.
23. O. Toprakci, H. A. K. Toprakci, L. W. Ji and X. W. Zhang, *KONA Powder Part. J.*, 2010, 50-73.
24. Y. Wang, P. He and H. Zhou, *Energy & Environmental Science*, 2011, **4**, 805-817.
25. L.-X. Yuan, Z.-H. Wang, W.-X. Zhang, X.-L. Hu, J.-T. Chen, Y.-H. Huang and J. B. Goodenough, *Energy & Environmental Science*, 2011, **4**, 269-284.
26. W.-J. Zhang, *J Power Sources*, 2011, **196**, 2962-2970.
27. D. Jugović and D. Uskoković, *J Power Sources*, 2009, **190**, 538-544.
28. J. Wang and X. Sun, *Energy & Environmental Science*, 2012, **5**, 5163-5185.
29. A. K. Padhi, K. S. Nanjundaswamy and J. B. Goodenough, *J Electrochem Soc*, 1997, **144**, 1188-1194.
30. H. Huang, S.-C. Yin and L. F. Nazar, *Electrochem Solid St*, 2001, **4**, A170-A172.
31. N. Ravet, Y. Chouinard, J. F. Magnan, S. Besner, M. Gauthier and M. Armand, *J Power Sources*, 2001, **97–98**, 503-507.
32. S.-Y. Chung, J. T. Bloking and Y.-M. Chiang, *Nat Mater*, 2002, **1**, 123-128.
33. C. Delacourt, P. Poizot, S. Levasseur and C. Masquelier, *Electrochem Solid St*, 2006, **9**, A352-A355.
34. P. Gibot, M. Casas-Cabanas, L. Laffont, S. Levasseur, P. Carlach, S. Hamelet, J.-M. Tarascon and C. Masquelier, *Nat Mater*, 2008, **7**, 741-747.
35. N. Meethong, H.-Y. S. Huang, W. C. Carter and Y.-M. Chiang, *Electrochem Solid St*, 2007, **10**, A134-A138.
36. J. Gaubicher, T. Le Mercier, Y. Chabre, J. Angenault and M. Quarton, *J Electrochem Soc*, 1999, **146**, 4375-4379.
37. T. A. Kerr, J. Gaubicher and L. F. Nazar, *Electrochem Solid St*, 2000, **3**, 460-462.
38. C. Delacourt, L. Laffont, R. Bouchet, C. Wurm, J.-B. Leriche, M. Morcrette, J.-M. Tarascon and C. Masquelier, *J Electrochem Soc*, 2005, **152**, A913-A921.
39. C. Delacourt, P. Poizot, M. Morcrette, J. M. Tarascon and C. Masquelier, *Chem Mater*, 2003, **16**, 93-99.
40. G. Li, H. Azuma and M. Tohda *Electrochem Solid St*, 2002, **5**, A135-A137.
41. K. Amine, H. Yasuda and M. Yamachi, *Electrochem Solid St*, 2000, **3**, 178-179.
42. J. Yang and J. J. Xu, *J Electrochem Soc*, 2006, **153**, A716-A723.
43. *History of Phostech Lithium*, http://www.phostechlithium.com/prf_historique_e.php, Accessed September 11, 2012.
44. *Süd-Chemie invests EUR 60 million in series production of the battery material lithium iron phosphate for electric vehicle drives (July 12, 2010)*, http://www.sud-chemie.com/scmcms/web/content.jsp?nodeId=7560, Accessed September 11, 2012.
45. *BASF signs licensing agreement to acquire Lithium Iron Phosphate (LFP) technology from LiFePO4+C (March 14, 2012)*, http://www.basf.com/group/corporate/de/news-and-media-relations/news-releases/news-releases-usa/P-12-059, Accessed September 11, 2012.
46. *Süd-Chemie and LG Chem to jointly manufacture high quality LFP (December 13, 2011)*, http://www.sud-chemie.com/scmcms/web/content.jsp?nodeId=7826, Accessed September 11, 2012.
47. *Nanophosphate® Lithium Iron Phosphate Battery Technology*, http://www.a123systems.com/lithium-iron-phosphate-battery.htm, Accessed September 11, 2012.
48. J. Barker, M. Y. Saidi and J. L. Swoyer *Electrochem Solid St*, 2003, **6**, A53-A55.
49. *Saft develops Super-Phosphate$^{TM}$ technology for rigorous defense applications (November 2, 2009)*, http://www.saftbatteries.com/SAFT/UploadedFiles/PressOffice/2009/CP_61-09_en.pdf, Accessed September 11, 2012.
50. *A123 Systems, Hydro-Québec, and the University of Texas Settle Lithium Metal Phosphate Battery Chemistry Patent Dispute (October 31, 2011)*, http://www.hydroquebec.com/transportation-electrification/pdf/communique-hq_2011-10-31.pdf, Accessed September 11, 2012.

51. *Valence Technology Settles Patent Dispute With Hydro-Quebec (June 13, 2012)*, http://ir.valence.com/releasedetail.cfm?ReleaseID=682776, Accessed September 11, 2012.
52. *A123 Systems Expands Portfolio of Grid Storage Solutions (May 1, 2012)*, http://www.a123systems.com/805ab788-d9a1-4518-9884-91aa2de0b3f5/media-room-2012-press-releases-detail.htm, Accessed September 11, 2012.
53. *A123 Systems Introduces Advanced Lithium Ion Battery Designed Specifically for Military Vehicle Applications (February 21, 2012)*, http://www.a123systems.com/14c75767-1afd-472b-b8df-e7a8dee023eb/media-room-2012-press-releases-detail.htm, Accessed September 11, 2012.
54. Z. Yang, D. Choi, S. Kerisit, K. M. Rosso, D. Wang, J. Zhang, G. Graff and J. Liu, *J Power Sources*, 2009, **192**, 588-598.
55. G.-N. Zhu, Y.-G. Wang and Y.-Y. Xia, *Energy & Environmental Science*, 2012, **5**, 6652-6667.
56. T. Ohzuku, A. Ueda and N. Yamamoto, *J Electrochem Soc*, 1995, **142**, 1431-1435.
57. E. Ferg, R. J. Gummow, A. de Kock and M. M. Thackeray, *J Electrochem Soc*, 1994, **141**, L147-L150.
58. L. Kavan and M. Grätzel, *Electrochem Solid St*, 2002, **5**, A39-A42.
59. L. Kavan, J. Procházka, T. M. Spitler, M. Kalbáč, M. Zukalová, T. Drezen and M. Grätzel, *J Electrochem Soc*, 2003, **150**, A1000-A1007.
60. *Altairnano: Solutions*, http://www.altairnano.com/solutions/, Accessed September 11, 2012.
61. *Hydro-Québec and Technifin form partnership to license lithium titanate spinel oxide (LTO) (October 20, 2011)*, http://www.hydroquebec.com/4d_includes/of_interest/PcAN2011-137.htm, Accessed September 11, 2012.
62. *High Performance Battery Materials: Lithium Titanate*, http://www.neicorporation.com/high_performance.html, Accessed September 11, 2012.
63. S. Y. Huang, L. Kavan, I. Exnar and M. Grätzel, *J Electrochem Soc*, 1995, **142**, L142-L144.
64. V. Luca, T. L. Hanley, N. K. Roberts and R. F. Howe, *Chem Mater*, 1999, **11**, 2089-2102.
65. C. Natarajan, K. Setoguchi and G. Nogami, *Electrochim Acta*, 1998, **43**, 3371-3374.
66. X. P. Gao, Y. Lan, H. Y. Zhu, J. W. Liu, Y. P. Ge, F. Wu and D. Y. Song, *Electrochem Solid St*, 2005, **8**, A26-A29.
67. J. Li, Z. Tang and Z. Zhang, *Electrochem Solid St*, 2005, **8**, A316-A319.
68. A. R. Armstrong, G. Armstrong, J. Canales and P. G. Bruce, *J Power Sources*, 2005, **146**, 501-506.
69. A. R. Armstrong, G. Armstrong, J. Canales, R. García and P. G. Bruce, *Adv Mater*, 2005, **17**, 862-865.
70. G. Armstrong, A. R. Armstrong, J. Canales and P. G. Bruce, *Electrochem Solid St*, 2006, **9**, A139-A143.
71. G. G. Amatucci and N. Pereira, *Journal of Fluorine Chemistry*, 2007, **128**, 243-262.
72. P. Poizot, S. Laruelle, S. Grugeon, L. Dupont and J. M. Tarascon, *Nature*, 2000, **407**, 496-499.
73. R. Malini, U. Uma, T. Sheela, M. Ganesan and N. Renganathan, *Ionics*, 2009, **15**, 301-307.
74. J. Cabana, L. Monconduit, D. Larcher and M. R. Palacín, *Adv Mater*, 2010, **22**, E170-E192.
75. M. M. Thackeray, W. I. F. David and J. B. Goodenough, *Materials Research Bulletin*, 1982, **17**, 785-793.
76. D. Larcher, G. Sudant, J.-B. Leriche, Y. Chabre and J.-M. Tarascon, *J Electrochem Soc*, 2002, **149**, A234-A241.
77. S. Grugeon, S. Laruelle, R. Herrera-Urbina, L. Dupont, P. Poizot and J.-M. Tarascon, *J Electrochem Soc*, 2001, **148**, A285-A292.
78. Z. Yuan, F. Huang, C. Feng, J. Sun and Y. Zhou, *Materials Chemistry and Physics*, 2003, **79**, 1-4.
79. Y. Li, B. Tan and Y. Wu, *Nano Letters*, 2007, **8**, 265-270.
80. K. T. Nam, D. W. Kim, P. J. Yoo, C. Y. Chiang, N. Meethong, P. T. Hammond, Y. M. Chiang and A. M. Belcher, *Science*, 2006, **312**, 885-888.

81. K. M. Shaju, F. Jiao, A. Debart and P. G. Bruce, *Physical Chemistry Chemical Physics*, 2007, **9**, 1837-1842.
82. W.-M. Zhang, X.-L. Wu, J.-S. Hu, Y.-G. Guo and L.-J. Wan, *Advanced Functional Materials*, 2008, **18**, 3941-3946.
83. Z.-M. Cui, L.-Y. Jiang, W.-G. Song and Y.-G. Guo, *Chem Mater*, 2009, **21**, 1162-1166.
84. T. Muraliganth, A. Vadivel Murugan and A. Manthiram, *Chemical Communications*, 2009, 7360-7362.
85. C. Ban, Z. Wu, D. T. Gillaspie, L. Chen, Y. Yan, J. L. Blackburn and A. C. Dillon, *Adv Mater*, 2010, **22**, E145-E149.
86. M. V. Reddy, T. Yu, C. H. Sow, Z. X. Shen, C. T. Lim, G. V. Subba Rao and B. V. R. Chowdari, *Advanced Functional Materials*, 2007, **17**, 2792-2799.
87. J. Liu, Y. Li, H. Fan, Z. Zhu, J. Jiang, R. Ding, Y. Hu and X. Huang, *Chem Mater*, 2009, **22**, 212-217.
88. H. Wang, L.-F. Cui, Y. Yang, H. Sanchez Casalongue, J. T. Robinson, Y. Liang, Y. Cui and H. Dai, *Journal of the American Chemical Society*, 2010, **132**, 13978-13980.
89. F. Badway, N. Pereira, F. Cosandey and G. G. Amatucci, *J Electrochem Soc*, 2003, **150**, A1209-A1218.
90. I. Plitz, F. Badway, J. Al-Sharab, A. DuPasquier, F. Cosandey and G. G. Amatucci, *J Electrochem Soc*, 2005, **152**, A307-A315.
91. N. Pereira, F. Badway, M. Wartelsky, S. Gunn and G. G. Amatucci, *J Electrochem Soc*, 2009, **156**, A407-A416.
92. A. N. Dey, *J Electrochem Soc*, 1971, **118**, 1547-1549.
93. D. Larcher, S. Beattie, M. Morcrette, K. Edstrom, J.-C. Jumas and J.-M. Tarascon, *J Mater Chem*, 2007, **17**, 3759-3772.
94. C. M. Park, J. H. Kim, H. Kim and H. J. Sohn, *Chem Soc Rev*, 2010, **39**, 3115-3141.
95. W.-J. Zhang, *J Power Sources*, 2011, **196**, 13-24.
96. W.-J. Zhang, *J Power Sources*, 2011, **196**, 877-885.
97. J. Wang, P. King and R. A. Huggins, *Solid State Ionics*, 1986, **20**, 185-189.
98. J. R. Szczech and S. Jin, *Energy & Environmental Science*, 2011, **4**, 56-72.
99. U. Kasavajjula, C. Wang and A. J. Appleby, *J Power Sources*, 2007, **163**, 1003-1039.
100. H. Li, X. J. Huang, L. Q. Chen, Z. G. Wu and Y. Liang, *Electrochem Solid St*, 1999, **2**, 547-549.
101. J. Graetz, C. C. Ahn, R. Yazami and B. Fultz, *Electrochem Solid St*, 2003, **6**, A194-A197.
102. J. P. Maranchi, A. F. Hepp, A. G. Evans, N. T. Nuhfer and P. N. Kumta, *J Electrochem Soc*, 2006, **153**, A1246-A1253.
103. S. Ohara, J. Suzuki, K. Sekine and T. Takamura, *J Power Sources*, 2004, **136**, 303-306.
104. T. Takamura, S. Ohara, M. Uehara, J. Suzuki and K. Sekine, *J Power Sources*, 2004, **129**, 96-100.
105. B. Gao, S. Sinha, L. Fleming and O. Zhou, *Adv Mater*, 2001, **13**, 816-819.
106. H. Li, X. Huang, L. Chen, G. Zhou, Z. Zhang, D. Yu, Y. Jun Mo and N. Pei, *Solid State Ionics*, 2000, **135**, 181-191.
107. C. K. Chan, H. Peng, G. Liu, K. McIlwrath, X. F. Zhang, R. A. Huggins and Y. Cui, *Nat Nano*, 2008, **3**, 31-35.
108. R. Ruffo, S. S. Hong, C. K. Chan, R. A. Huggins and Y. Cui, *The Journal of Physical Chemistry C*, 2009, **113**, 11390-11398.
109. H. Kim, M. Seo, M.-H. Park and J. Cho, *Angewandte Chemie International Edition*, 2010, **49**, 2146-2149.
110. X. H. Liu, L. Q. Zhang, L. Zhong, Y. Liu, H. Zheng, J. W. Wang, J.-H. Cho, S. A. Dayeh, S. T. Picraux, J. P. Sullivan, S. X. Mao, Z. Z. Ye and J. Y. Huang, *Nano Letters*, 2011, **11**, 2251-2258.
111. *Nexeon Technology Overview*, http://www.nexeon.co.uk/technology/, Accessed August 28, 2012.
112. M. Green, E. Fielder, B. Scrosati, M. Wachtler and J. S. Moreno, *Electrochem Solid St*, 2003, **6**, A75-A79.

113. *3M™ Battery Anode*, http://solutions.3m.com/wps/portal/3M/en_US/ElectronicsChemicals/Home/Products/BatteryMaterials/BatteryAnode/, Accessed August 28, 2012.
114. *Amprius, Inc.*, http://www.amprius.com, Accessed September 17, 2012.
115. M. Winter and J. O. Besenhard, *Electrochim Acta*, 1999, **45**, 31-50.
116. M. Noh, Y. Kim, M. G. Kim, H. Lee, H. Kim, Y. Kwon, Y. Lee and J. Cho, *Chem Mater*, 2005, **17**, 3320-3324.
117. J. Yang, M. Winter and J. O. Besenhard, *Solid State Ionics*, 1996, **90**, 281-287.
118. C. Kim, M. Noh, M. Choi, J. Cho and B. Park, *Chem Mater*, 2005, **17**, 3297-3301.
119. N. C. Li and C. R. Martin, *J Electrochem Soc*, 2001, **148**, A164-A170.
120. X. F. Lei, C. W. Wang, Z. H. Yi, Y. G. Liang and J. T. Sun, *J Alloy Compd*, 2007, **429**, 311-315.
121. N. S. Hudak and D. L. Huber, *J Electrochem Soc*, 2012, **159**, A688-A695.
122. Y. Liu, N. S. Hudak, D. L. Huber, S. J. Limmer, J. P. Sullivan and J. Y. Huang, *Nano Letters*, 2011, **11**, 4188-4194.
123. C. Y. Wang, Y. S. Meng, G. Ceder and Y. Li, *J Electrochem Soc*, 2008, **155**, A615-A622.
124. Z. Y. Wang, Y. Li and J. Y. Lee, *Electrochem Commun*, 2009, **11**, 1179-1182.
125. Q. Fan, P. J. Chupas and M. S. Whittingham, *Electrochem Solid St*, 2007, **10**, A274-A278.
126. P. P. Ferguson, R. A. Dunlap and J. R. Dahn, *J Electrochem Soc*, 2010, **157**, A326-A332.
127. X.-L. Wang, W.-Q. Han, J. Chen and J. Graetz, *ACS Applied Materials & Interfaces*, 2010, **2**, 1548-1551.
128. *SONY's New Nexelion Hybrid Lithium Ion Batteries to Have Thirty-Percent More Capacity Than Conventional Offering (February 15, 2005)*, http://www.sony.net/SonyInfo/News/Press/200502/05-006E/, Accessed August 28, 2012.
129. *SONY has adopted the amorphous tin-based negative electrode for the PC market (July 12, 2011)*, http://www.sony.co.jp/SonyInfo/News/Press/201107/11-078/, Accessed August 28, 2012.
130. N. A. Kaskhedikar and J. Maier, *Adv Mater*, 2009, **21**, 2664-2680.
131. D. S. Su and R. Schlögl, *ChemSusChem*, 2010, **3**, 136-168.
132. B. J. Landi, M. J. Ganter, C. D. Cress, R. A. DiLeo and R. P. Raffaelle, *Energy & Environmental Science*, 2009, **2**, 638-654.
133. B. Gao, C. Bower, J. D. Lorentzen, L. Fleming, A. Kleinhammes, X. P. Tang, L. E. McNeil, Y. Wu and O. Zhou, *Chemical Physics Letters*, 2000, **327**, 69-75.
134. B. Gao, A. Kleinhammes, X. P. Tang, C. Bower, L. Fleming, Y. Wu and O. Zhou, *Chemical Physics Letters*, 1999, **307**, 153-157.
135. A. S. Claye, J. E. Fischer, C. B. Huffman, A. G. Rinzler and R. E. Smalley, *J Electrochem Soc*, 2000, **147**, 2845-2852.
136. E. Frackowiak, S. Gautier, H. Gaucher, S. Bonnamy and F. Beguin, *Carbon*, 1999, **37**, 61-69.
137. F. Leroux, K. Méténier, S. Gautier, E. Frackowiak, S. Bonnamy and F. Béguin, *J Power Sources*, 1999, **81–82**, 317-322.
138. G. T. Wu, C. S. Wang, X. B. Zhang, H. S. Yang, Z. F. Qi, P. M. He and W. Z. Li, *J Electrochem Soc*, 1999, **146**, 1696-1701.
139. C. Masarapu, V. Subramanian, H. W. Zhu and B. Q. Wei, *Advanced Functional Materials*, 2009, **19**, 1008-1014.
140. Y. Liu, H. Zheng, X. H. Liu, S. Huang, T. Zhu, J. Wang, A. Kushima, N. S. Hudak, X. Huang, S. Zhang, S. X. Mao, X. Qian, J. Li and J. Y. Huang, *ACS Nano*, 2011, **5**, 7245-7253.
141. S.-H. Yoon, C.-W. Park, H. Yang, Y. Korai, I. Mochida, R. T. K. Baker and N. M. Rodriguez, *Carbon*, 2004, **42**, 21-32.
142. C. Kim, K. S. Yang, M. Kojima, K. Yoshida, Y. J. Kim, Y. A. Kim and M. Endo, *Advanced Functional Materials*, 2006, **16**, 2393-2397.
143. J. Liwen and Z. Xiangwu, *Nanotechnology*, 2009, **20**, 155705.
144. M. H. Liang and L. J. Zhi, *J Mater Chem*, 2009, **19**, 5871-5878.
145. M. Pumera, *Energy & Environmental Science*, 2011, **4**, 668-674.

146. D. A. C. Brownson, D. K. Kampouris and C. E. Banks, *J Power Sources*, 2011, **196**, 4873-4885.
147. A. Abouimrane, O. C. Compton, K. Amine and S. T. Nguyen, *Journal of Physical Chemistry C*, 2010, **114**, 12800-12804.
148. P. Guo, H. H. Song and X. H. Chen, *Electrochem Commun*, 2009, **11**, 1320-1324.
149. G. X. Wang, X. P. Shen, J. Yao and J. Park, *Carbon*, 2009, **47**, 2049-2053.
150. T. Bhardwaj, A. Antic, B. Pavan, V. Barone and B. D. Fahlman, *Journal of the American Chemical Society*, 2010, **132**, 12556-12558.
151. E. Yoo, J. Kim, E. Hosono, H. Zhou, T. Kudo and I. Honma, *Nano Letters*, 2008, **8**, 2277-2282.
152. X. F. Zhou, F. Wang, Y. M. Zhu and Z. P. Liu, *J Mater Chem*, 2011, **21**, 3353-3358.
153. L. Dimesso, C. Forster, W. Jaegermann, J. P. Khanderi, H. Tempel, A. Popp, J. Engstler, J. J. Schneider, A. Sarapulova, D. Mikhailova, L. A. Schmitt, S. Oswald and H. Ehrenberg, *Chem Soc Rev*, 2012, **41**, 5068-5080.
154. B. Hertzberg, A. Alexeev and G. Yushin, *Journal of the American Chemical Society*, 2010, **132**, 8548-8549.
155. H. Kim and J. Cho, *Nano Letters*, 2008, **8**, 3688-3691.
156. L.-F. Cui, Y. Yang, C.-M. Hsu and Y. Cui, *Nano Letters*, 2009, **9**, 3370-3374.
157. J. Lee, J. Bae, J. Heo, I. T. Han, S. N. Cha, D. K. Kim, M. Yang, H. S. Han, W. S. Jeon and J. Chung, *J Electrochem Soc*, 2009, **156**, A905-A910.
158. Y. Yu, L. Gu, C. Zhu, P. A. van Aken and J. Maier, *Journal of the American Chemical Society*, 2009, **131**, 15984-15985.
159. Y. Yu, L. Gu, C. Wang, A. Dhanabalan, P. A. van Aken and J. Maier, *Angewandte Chemie*, 2009, **121**, 6607-6611.
160. T. Prem Kumar, R. Ramesh, Y. Y. Lin and G. T.-K. Fey, *Electrochem Commun*, 2004, **6**, 520-525.
161. G. Cui, Y.-S. Hu, L. Zhi, D. Wu, I. Lieberwirth, J. Maier and K. Müllen, *Small*, 2007, **3**, 2066-2069.
162. W.-M. Zhang, J.-S. Hu, Y.-G. Guo, S.-F. Zheng, L.-S. Zhong, W.-G. Song and L.-J. Wan, *Adv Mater*, 2008, **20**, 1160-1165.
163. J. Hassoun, G. Derrien, S. Panero and B. Scrosati, *Adv Mater*, 2008, **20**, 3169-3175.
164. S. M. Paek, E. Yoo and I. Honma, *Nano Letters*, 2009, **9**, 72-75.
165. X. Y. Wang, X. F. Zhou, K. Yao, J. G. Zhang and Z. P. Liu, *Carbon*, 2011, **49**, 133-139.
166. L. Zhi, Y.-S. Hu, B. E. Hamaoui, X. Wang, I. Lieberwirth, U. Kolb, J. Maier and K. Müllen, *Adv Mater*, 2008, **20**, 1727-1731.
167. X. J. Zhu, Y. W. Zhu, S. Murali, M. D. Stollers and R. S. Ruoff, *ACS Nano*, 2011, **5**, 3333-3338.

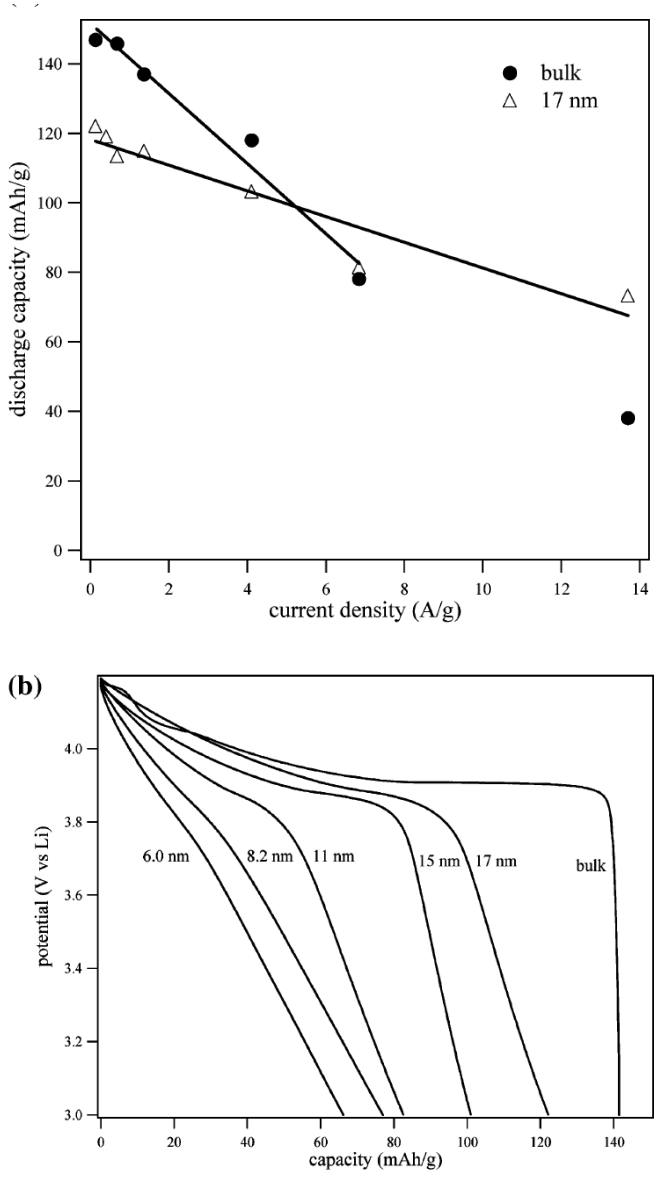


**Figure 1.** (a) Rate capability of nanocrystalline and bulk $LiCoO_2$ at various discharge rates (1-100 C rate). Solid lines are fitted results. (b) Crystallite size dependence of the second lithiation potential curves for $LiCoO_2$. Adapted with permission from *Journal of the American Chemical Society*, Okubo et al., Volume 129, Pages 7444–7452. Copyright 2007 American Chemical Society. http://dx.doi.org/10.1021/ja0681927

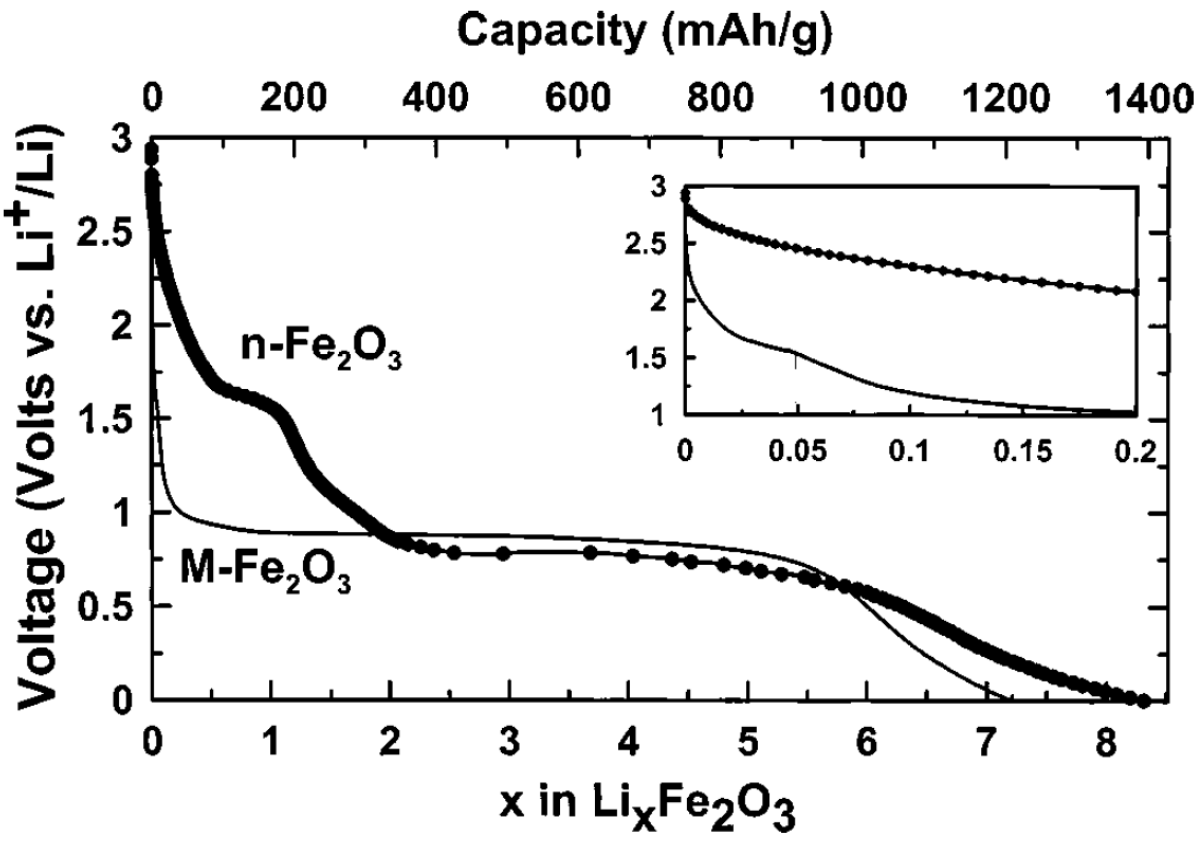


**Figure 2.** Voltage-composition curves for lithiation of nano-$Fe_2O_3$ and bulk $Fe_2O_3$ ("M-$Fe_2O_3$") hematite samples. The zoom in the inset shows a small 1.6-V plateau for bulk $Fe_2O_3$. *Rate*: 1 Li per formula unit in 5 h at 25°C. Reproduced by permission of The Electrochemical Society from *Journal of The Electrochemical Society*, D. Larcher et al., Volume 150, Pages A133-A139, Copyright 2003. http://dx.doi.org/10.1149/1.1528941

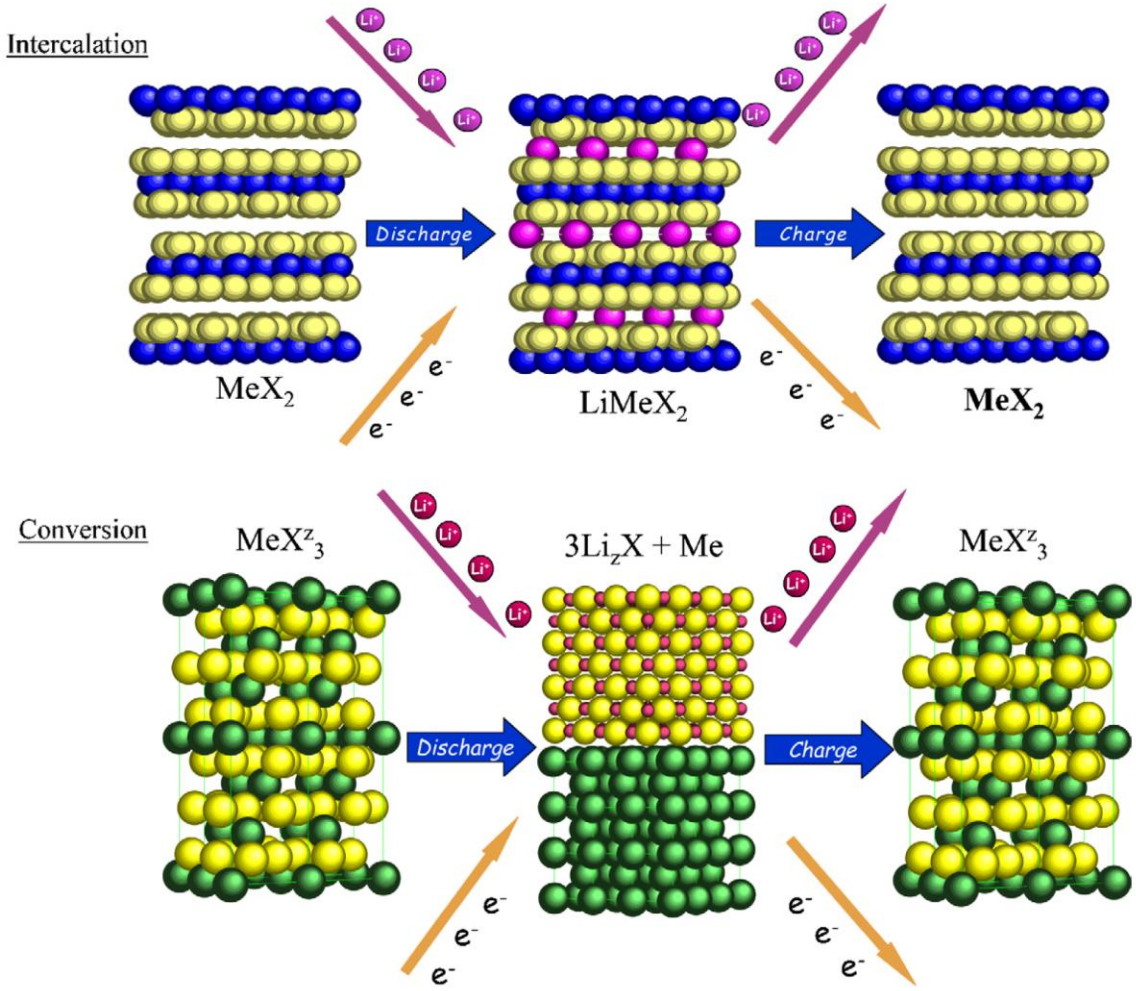


**Figure 3.** Differing crystallographic reaction mechanisms (intercalation and conversion) occurring in the active materials of electrodes during battery charge or discharge. The intercalation reaction typically involves at most 1 electron transfer per metal atom (typically <250 mAh/g) whereas the conversion reaction can involve as many as 3 electrons transferred per metal atom (typically >700 mAh/g). Reprinted from *Journal of Fluorine Chemistry*, Volume 128, G. Amatucci and N. Pereira, "Fluoride based electrode materials for advanced energy storage devices", Pages 243-262, Copyright 2007, with permission from Elsevier.
http://dx.doi.org/10.1016/j.jfluchem.2006.11.016

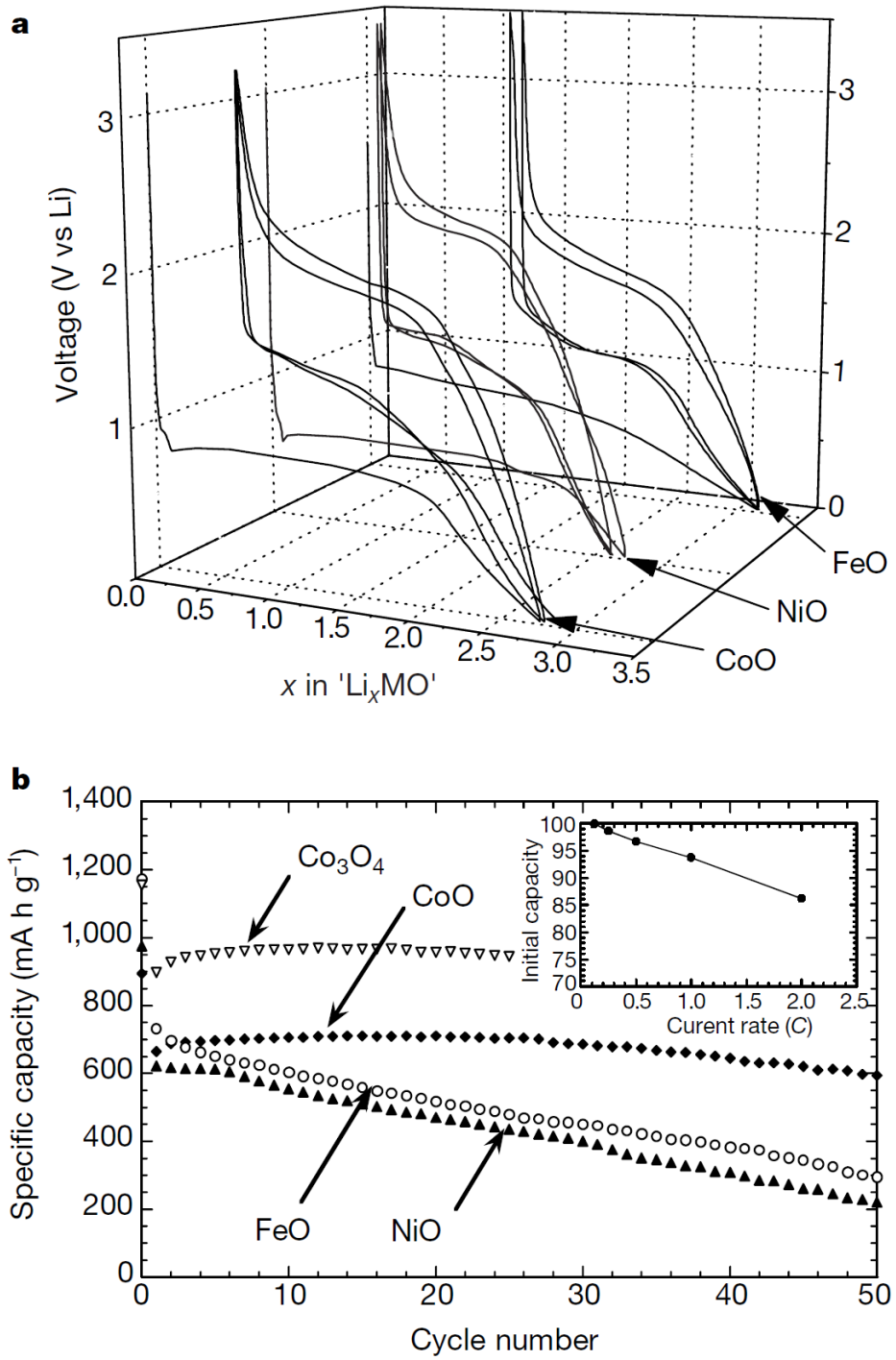


**Figure 4.** Properties of lithium cells with metal oxide conversion electrodes. **(a)** The voltage vs. composition profile for various cells cycled between 0.01 V and 3 V (vs. $Li/Li^+$) at a rate of C/5 (1 lithium ion per metal atom in 5 hours). **(b)** Cycling capacity for the same cells (including a $Co_3O_4$/Li cell) under similar conditions. Inset: the rate capability of a CoO electrode. Reprinted by permission from Macmillan Publishers Ltd: *Nature*, Volume 407, Pages 496-499, copyright 2000.
http://dx.doi.org/10.1038/35035045

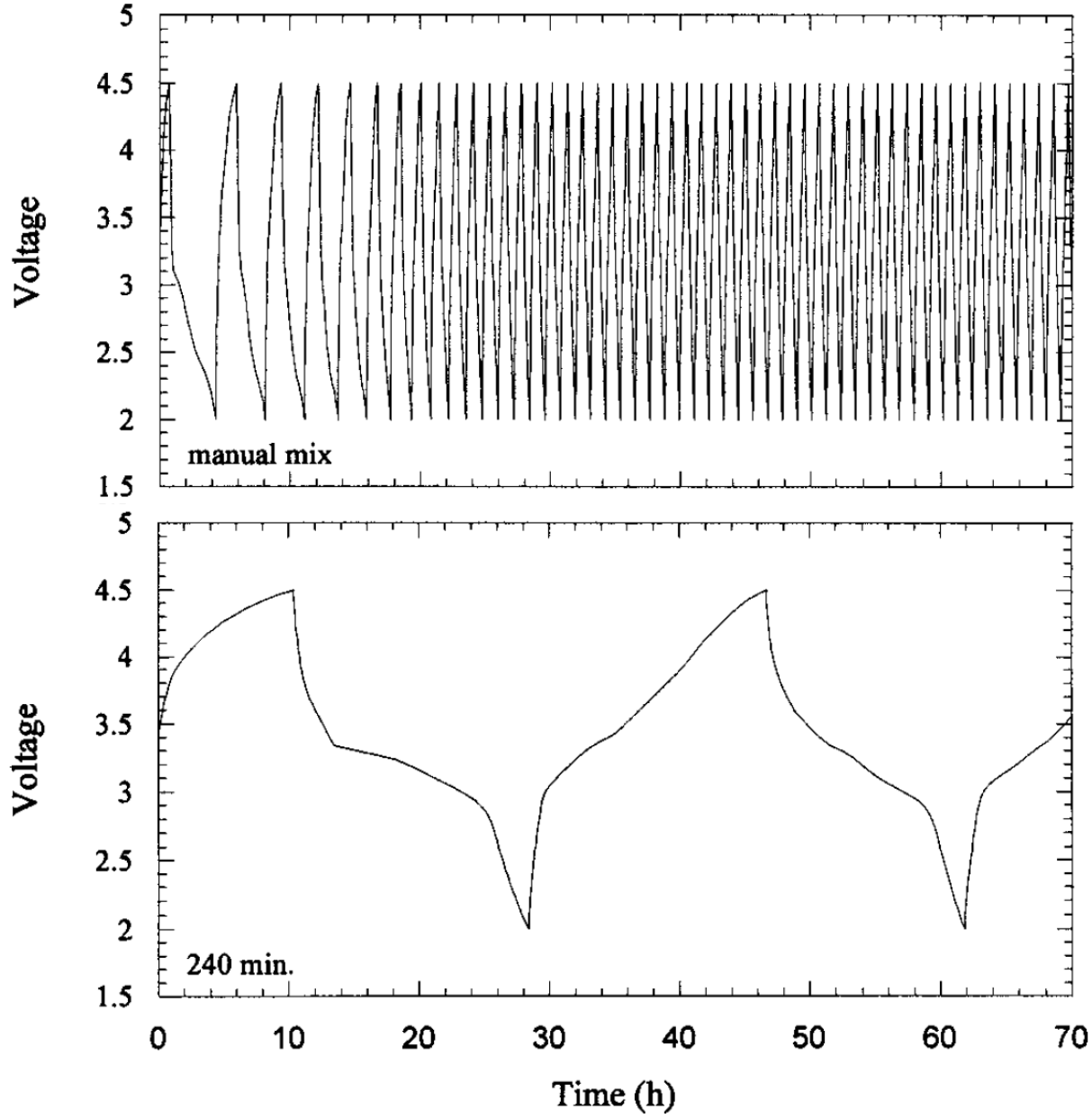


**Figure 5.** Voltage *vs.* time plots for Li | $LiPF_6$ in EC:DMC | $FeF_3$:C cells cycled at 7.58 mA $g^{-1}_{composite}$ as a function of milling time. "Manual mix" sample had a crystallite size of 102 nm, and "240 min." sample had a crystallite size of 25 nm. Reproduced by permission of The Electrochemical Society from *Journal of The Electrochemical Society*, F. Badway et al., Volume 150, Pages A1209-A1218, Copyright 2003. http://dx.doi.org/10.1149/1.1596162

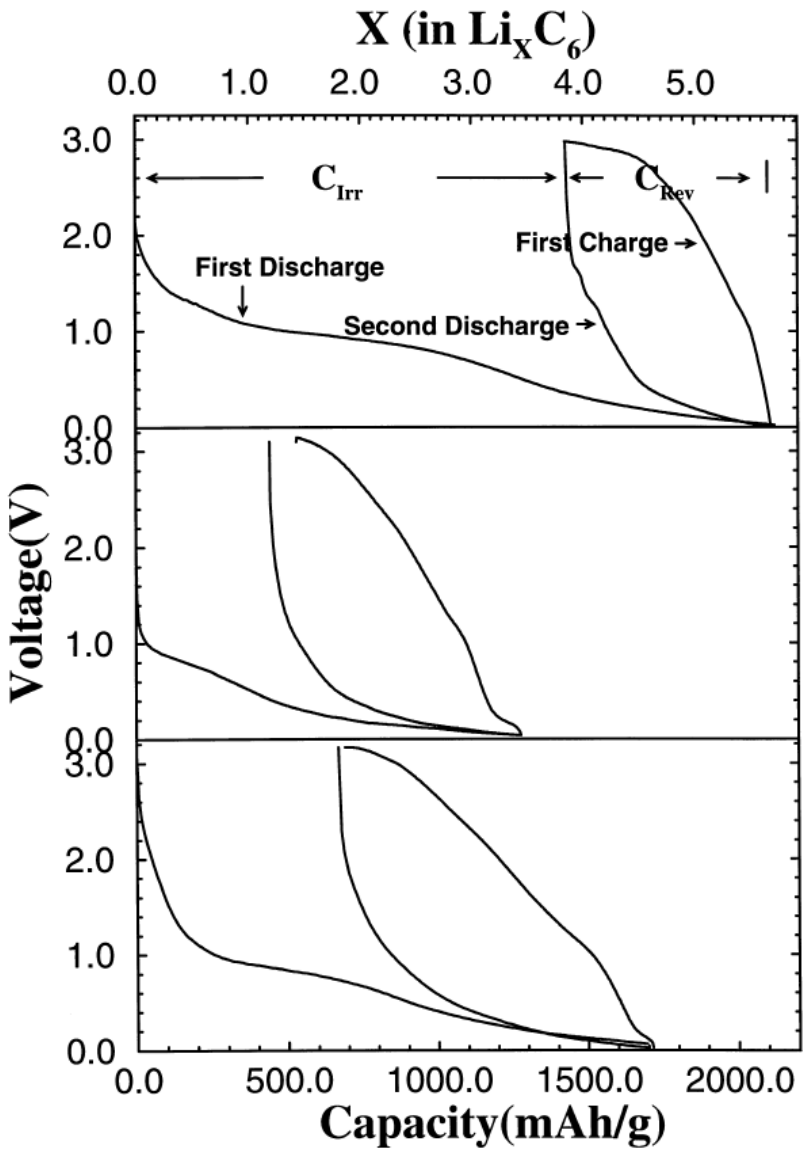


**Figure 6.** Electrochemical lithiation/de-lithiation of SWNT electrodes: effect of sample treatment on potential profile. *Top*: purified SWNT. *Middle*: SWNT ball-milled for 1 minute. *Bottom*: SWNT ball-milled for 10 minutes. The data were collected at a constant current 50 mA $g^{-1}$. Reprinted from *Chemical Physics Letters*, Volume 327, B. Gao et al., "Enhanced saturation lithium composition in ball-milled single-walled carbon nanotubes", Pages 69-75, Copyright 2000, with permission from Elsevier. http://dx.doi.org/10.1016/S0009-2614(00)00851-4

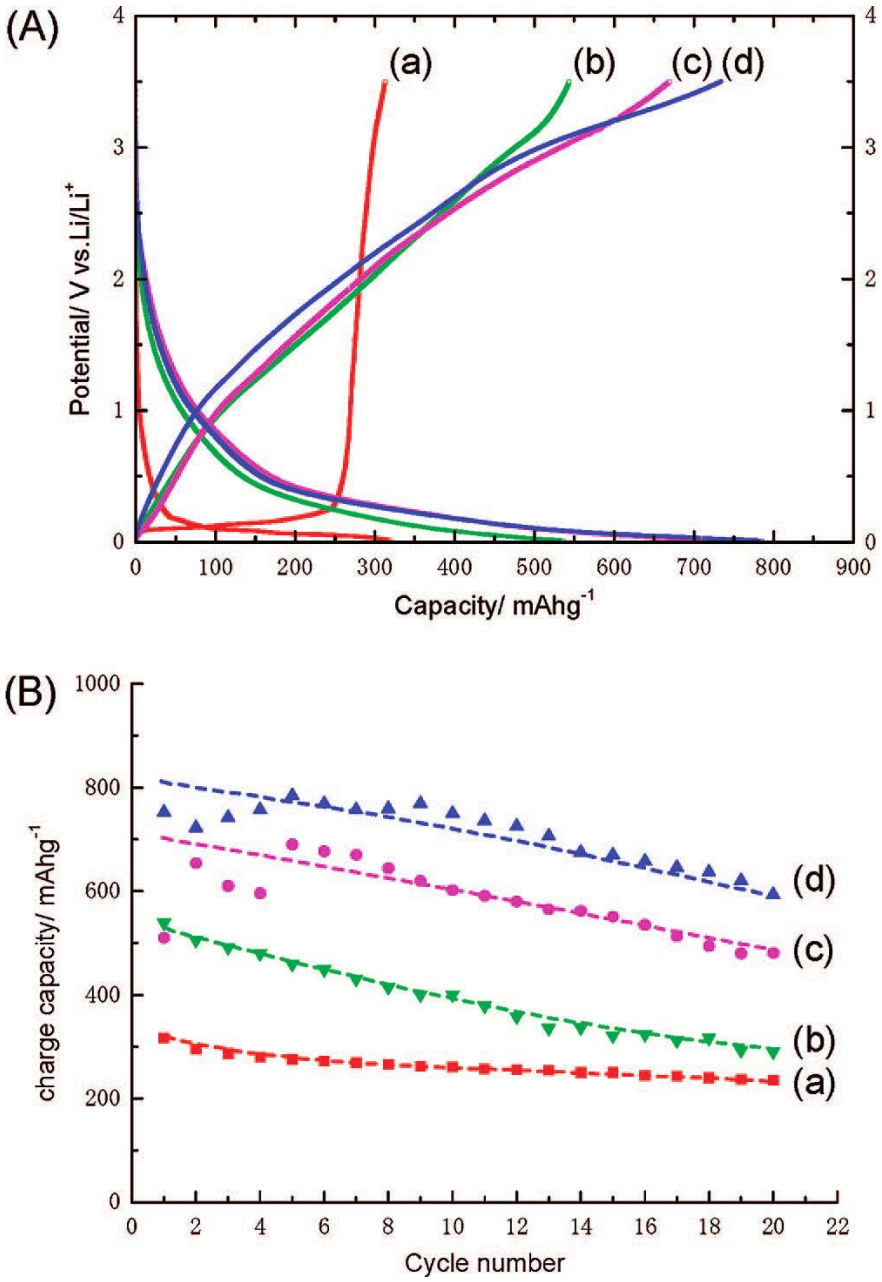


**Figure 7**. Lithium insertion/extraction properties of graphene and related materials. (A) charge/discharge profiles and (B) cycling performance of (a) graphite, (b) graphene, (c) graphene + carbon nanotube, and (d) graphene + fullerene $C_{60}$. Specific current is 50 mA $g^{-1}$. Reprinted with permission from *Nano Letters*, Yoo et al., Volume 8, Pages 2277-2282. Copyright 2008 American Chemical Society. http://dx.doi.org/10.1021/nl800957b